Incoherent-light temporal stretching of high-speed intensity waveforms

Bo Li* and José Azaña

Institut National de la Recherche Scientifique—Energie, Matériaux et Télécommunications, Montréal, Québec H5A 1K6, Canada
**Corresponding author: bo.li@emt.inrs.ca*

Received April 23, 2014; revised June 10, 2014; accepted June 13, 2014;
posted June 17, 2014 (Doc. ID 210649); published July 15, 2014

We propose and demonstrate experimentally the first incoherent-light scheme for temporal imaging (magnification) of intensity waveforms. The scheme is based on a time-domain equivalent of a pinhole camera under incoherent illumination, involving two dispersive lines and temporal intensity modulation with a short gate. We report incoherent-light temporal stretching of radiofrequency waveforms by a magnification factor of 2.86, with a time–bandwidth product exceeding 160, i.e., a resolution of ~50 ps over a temporal aperture of ~8 ns, totally avoiding the use of chirp-controlled pulsed lasers. This work opens up new perspectives for realization of many critical high-speed signal-processing modules using practical incoherent light-wave schemes.

OCIS codes: (070.1170) Analog optical signal processing; (110.6915) Time imaging; (250.4745) Optical processing devices; (320.7085) Ultrafast information processing.
http://dx.doi.org/10.1364/OL.39.004243

The space–time duality theory relies on the mathematical equivalence between the free-space diffraction of a spatial field and the chromatic dispersion of a temporal waveform [1–4]. This basic equivalence has been extended to the concept of a time lens [2–4], which is the temporal equivalent of a thin lens and can be implemented through quadratic temporal phase modulation. By suitably combining dispersion and time lenses, temporal imaging [1–4] and related concepts have been used for generation [1,5–7], measurement [2,3,8–10], cloaking [11], and processing [4,12] of time-domain waveforms, from electronic and radiofrequency (RF) signals [7,8,10,12] to ultrafast optical information [1–6,9,11]. The performance of time-lens-based systems, e.g., evaluated in the form of a time–bandwidth product (TBP), or the number of resolvable points, depends essentially on the time-lens frequency bandwidth [2–4]. For a moderate performance, time lenses can be realized using practical electro-optic phase modulation processes [2,6]. However, high-performance time-lens systems, e.g., offering TBPs >10, require the use of broadband (short-pulse) coherent light pulses, with bandwidths typically approaching or exceeding 10 nm, combined with precise control of the pulses' phase chirp [4,5,7–12]. Such requirements represent a critical hurdle to the practical development of temporal imaging systems [2–4,6,9,11] and related methods [5,7,8,10,12]. Thus, the possibility of implementing space–time duality concepts using an incoherent light-wave approach has attracted increased interest over the last few years [13–16]. Temporally incoherent light is inherently broadband and can be generally produced in a simpler and more affordable fashion than its coherent counterpart. Mechanisms have been demonstrated for temporal dispersion of incoherent optical waveforms [14–16]. However, no system requiring time lenses, e.g., a temporal imaging system, has been realized previously using an incoherent light-wave approach.

We report here the first practical scheme for temporal imaging of incoherent-light intensity waveforms, with TBPs around 160, avoiding the use of broadband pulsed laser sources and their coherent phase chirp control. The scheme is proved to be particularly useful for temporal stretching of high-speed RF waveforms, a functionality that has been investigated widely to adapt the bandwidth of RF signals to available detection or measurement instrumentation [7,8,10,12].

Figure 1(b) shows an illustration of the proposed scheme. Our approach is based on a time-domain equivalent of a classical pinhole camera illuminated by incoherent light [17], represented in Fig. 1(a). The idea of a temporal pinhole camera was first proposed and investigated by Kolner at the theoretical level [18]. However, for a coherent temporal pinhole camera, the system performance, particularly, the temporal aperture and

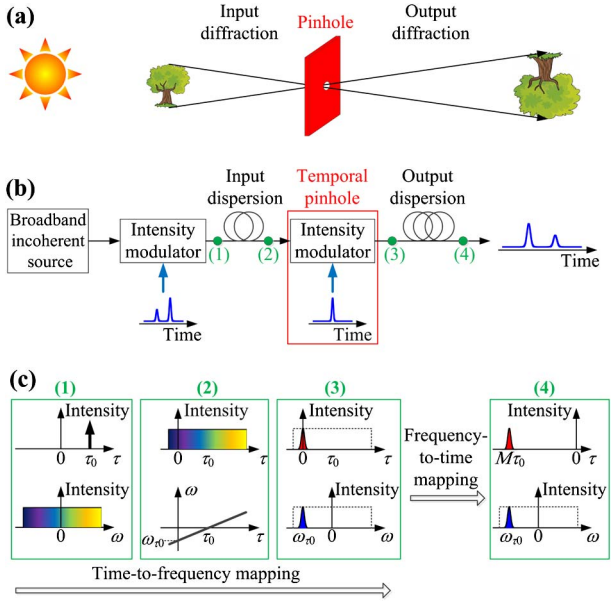

Fig. 1. (a) Illustration of an incoherent-light spatial imaging system (pinhole camera). (b) Proposed scheme for incoherent-light temporal imaging, which is constructed as the temporal equivalent of the incoherent-light pinhole camera. (c) Illustration of the impulse response of the temporal imaging system in (b), ignoring group delays. All represented temporal waveforms and spectra, and the instantaneous frequency curve, are averaged profiles.

the related TBP, is directly dependent on the input signal features (frequency bandwidth), thus being generally limited to processing ultrashort pulse waveforms [18]; to give an example, a temporal pinhole camera demonstrated recently exhibited relatively poor performance, with a TBP <10 [19]. We show here how the temporal pinhole concept holds the key for the development of incoherent-light temporal imaging and related systems with greatly improved performance. In relation to Fig. 1(b), light from a broadband, temporally incoherent optical source is modulated in intensity by the input waveform to be processed. The modulated light first propagates through a dispersive line, a medium or device providing a predominantly linear group-delay variation, with slope $\ddot{\Phi}_{\mathrm{In}}$, over the entire optical bandwidth. This is followed by temporal intensity modulation with a short pulse waveform, implementing the time-domain pinhole. The resulting modulated light wave is finally dispersed through a second dispersive line, characterized by a linear group delay with slope $\ddot{\Phi}_{\mathrm{Out}}$. The *averaged* optical intensity at the system output is a temporally scaled (magnified or compressed) image of the input intensity waveform.

The proposed incoherent temporal imaging process consists of two main steps, namely, time-to-frequency mapping of the input intensity waveform, implemented at the output of the temporal pinhole, followed by dispersion-induced frequency-to-time mapping. Time-to-frequency (frequency-to-time) mapping refers to a process by which the input temporal waveform (spectrum) is transferred into the output spectrum (temporal waveform). These two steps can be visualized easily through an analysis of the system temporal impulse response, as illustrated in Fig. 1(c). Assuming that the light source is totally incoherent (white noise), with a uniform energy spectrum, one can show that the incoherent system in Fig. 1(b) is linear in intensity, assuming averaging over multiple realizations [13,20]. As such, the system can be completely characterized by its response to a temporal impulse located at τ_0. The input dispersion maps the light source spectrum along the time domain in such a way that an averaged linear frequency chirp of slope $1/\ddot{\Phi}_{\mathrm{In}}$ is induced along the duration of the dispersed waveform. The pinhole modulation implements temporal filtering of the chirped light at a reference time, selecting in average a narrow portion of the original spectrum, centered at wavelength $\omega_{\tau 0}$, which is directly proportional to τ_0, i.e., $\omega_{\tau 0} = -\tau_0/\ddot{\Phi}_{\mathrm{In}}$. In this way, the predicted time-to-frequency mapping is performed. Considering that the output of the pinhole modulation process is a short pulse, frequency-to-time mapping is subsequently induced on this pulse by the output dispersion [14,15], with a scaling defined by $\ddot{\Phi}_{\mathrm{Out}}$. These combined processes lead to the anticipated impulse relocation at $M\tau_0$, where $M = -\ddot{\Phi}_{\mathrm{Out}}/\ddot{\Phi}_{\mathrm{In}}$ then defines the temporal magnification factor of the imaging system.

Similarly to its coherent counterpart, the performance of an incoherent temporal imaging system is described by its temporal resolution and aperture. The latter refers to the time window over which the desired imaging process is implemented. These two parameters are typically defined at the point of highest resolution in the system, namely, the input port for temporal magnification systems ($|M| > 1$).

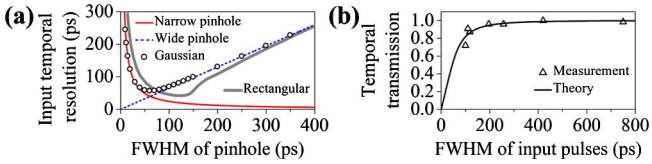

Fig. 2. Input resolution and transmission characteristic of the proposed temporal imaging scheme. (a) Numerically simulated input resolution as a function of the pinhole time-width, assuming a temporal pinhole with a Gaussian shape (black circles) and with a rectangular shape (solid gray thick curves), and the analytical approximations for the case of a narrow pinhole (solid red thin curves) and a wide pinhole (blue dotted curves). (b) Normalized peak intensity of the output temporal pulse for input Gaussian pulses of different time widths (experiments versus theory).

According to the statistical properties of a white-noise incoherent light source [13,20], the impulse response function of the incoherent temporal-imaging processes considered can be obtained by squaring the magnitude of the field impulse response of the corresponding coherent system [18]. Figure 2(a) shows the numerically simulated input temporal resolution of an *incoherent temporal magnification* system (black circles), assuming that the temporal pinhole has a Gaussian profile, input dispersion is −692 ps/nm and output dispersion is 1981 ps/nm (experimental setup data). In particular, for the proposed incoherent temporal magnification scheme, the output temporal resolution is estimated as the intensity full width at half-maximum (FWHM) of the time-domain impulse response (the time-domain pulse waveform at the system output when an ideal temporal impulse is launched at the system input). The corresponding input temporal resolution, which can be obtained through scaling by the magnification factor, i.e., $\delta\tau_{\mathrm{In}} = \delta\tau_{\mathrm{Out}}/|M|$, can be described analytically by two approximations:

$$\delta\tau_{\mathrm{In},n} \approx (4 \ln 2|\ddot{\Phi}_{\mathrm{In}}|)/\Delta T_P, \tag{1}$$

$$\delta\tau_{\mathrm{In},w} \approx \Delta T_P|1 + (\ddot{\Phi}_{\mathrm{In}}/\ddot{\Phi}_{\mathrm{Out}})|, \tag{2}$$

where ΔT_P holds for the intensity FWHM of the temporal pinhole. As illustrated in Fig. 2(a), Eqs. (1) and (2) provide a good approximation for the resolutions in the cases of a temporally narrow pinhole (solid red thin curve) and a wide pinhole (blue dotted curve), respectively. The approximation in Eq. (2) roughly corresponds to a direct projection of the temporal pinhole onto the output image, as expected for a pinhole duration that is sufficiently long to neglect the effect of dispersive propagation. The approximation in Eq. (1) corresponds to the opposite case, where a projection of the dispersion-induced temporal far-field (Fraunhofer) pattern of the pinhole is obtained onto the output image. Optimum output temporal resolution is achieved at the point where the two approximations coincide. In this case, the intensity FWHM of the pinhole should be fixed as

$$\Delta T_P \approx 2\sqrt{\ln 2|\ddot{\Phi}_{\mathrm{In}}\ddot{\Phi}_{\mathrm{Out}}/(\ddot{\Phi}_{\mathrm{In}}+\ddot{\Phi}_{\mathrm{Out}})|} \quad (3)$$

and the corresponding input temporal resolution is

$$\delta\tau_{\mathrm{In}} \approx \Delta T_P|1-(1/M)|. \quad (4)$$

Equation (4) shows that the system resolution approaches the pinhole time width for very high magnification factors ($|M| \gg 1$). Interestingly, for moderate-to-low magnification/compression factors, the system can be designed to provide an arbitrarily high resolution by simply using dispersive elements of opposite signs (with M being positive). Ideally, infinite resolution ($\delta\tau_{\mathrm{In}} = 0$) can be achieved for the trivial case when $M = 1$, requiring an infinitely long temporal pinhole (in practice, the pinhole full time width should exceed the duration of the dispersed input waveform). Considering that diffraction has only one sign, this possibility is not attainable in the space-domain case, where resolution is essentially limited by the pinhole extent [17,18]. Additionally, the resolution of the temporal imaging system can be improved further by using a pinhole with a different temporal shape, e.g., a rectangular pinhole, as shown in Fig. 2(a) (solid gray thick curve).

For an incoherent temporal imaging system with an optimum temporal pinhole defined by Eq. (3), the system response can be described mathematically as

$$\langle I_{\mathrm{Out}}(\tau)\rangle \propto I_{\mathrm{In}}\left(\frac{\tau}{M}\right) \otimes I_{\mathrm{Pinhole}}\left(\frac{\ddot{\Phi}_{\mathrm{In}}}{\ddot{\Phi}_{\mathrm{In}}+\ddot{\Phi}_{\mathrm{Out}}}\tau\right), \quad (5)$$

where we recall that $M = -\ddot{\Phi}_{\mathrm{Out}}/\ddot{\Phi}_{\mathrm{In}}$ is the temporal magnification factor; $I_{\mathrm{In}}(\tau)$, $I_{\mathrm{Pinhole}}(\tau)$, and $I_{\mathrm{Out}}(\tau)$ are the intensity temporal profiles of the input waveform, temporal pinhole, and output waveform, respectively; $\langle\cdot\rangle$ denotes averaging over multiple realizations; and $\otimes$ represents convolution. Figure 2(b) shows the normalized peak intensity of the output temporal pulse for input Gaussian pulses of different time widths, where the measured values (triangles) are compared with the theoretical transmission characteristic (black solid curve) calculated numerically by Eq. (5). In the calculation and experiment, the temporal pinhole is approximately rectangular with an intensity FWHM of ~146 ps [see Fig. 3(c)]. As expected, the intensity transmission deteriorates as the input pulse width is decreased below the corresponding resolution value. In particular, the estimated input resolution from Fig. 2(a) is ~51 ps, representing a threefold improvement over the pinhole width. The normalized transmission in Fig. 2(b) corresponding to this resolution exceeds ~55%.

In a practical setup, the uniform (infinite-bandwidth) energy spectrum of the ideal white-noise light source is emulated over a limited frequency bandwidth. This imposes a restriction on the system temporal aperture. As illustrated in Fig. 1(b), to ensure that some energy of the dispersed light pulse can pass through the pinhole, the input impulse must be within a certain time window (temporal aperture), i.e., $T_A = 2\pi|\ddot{\Phi}_{\mathrm{In}}|\Delta f_{\mathrm{Opt}}$, where Δf_{Opt} is the full-width optical bandwidth of the incoherent light source [18]. A similar figure applies to the coherent case, typically leading to a temporal aperture greatly constrained by the limited bandwidth of the input optical waveform to be imaged [19]. Notice that in the incoherent-light system, the temporal aperture is fully independent of the features (e.g., bandwidth) of the intensity signal to be processed.

Figure 3(a) shows the experimental setup and results for incoherent-light temporal magnification. Broadband incoherent light with a nearly uniform spectrum [~11.6 nm bandwidth and centered at a wavelength of 1549.9 nm; see Fig. 3(b)] is first generated by spectrally filtering the optical radiation from a superluminescent diode followed by amplification with a semiconductor optical amplifier. The input incoherent optical signal to be imaged is obtained by intensity modulation of the incoherent light with the RF waveform under analysis using a 40 GHz electro-optic intensity modulator. The RF waveform is generated by a 12 GHz electronic arbitrary waveform generator and then amplified by a

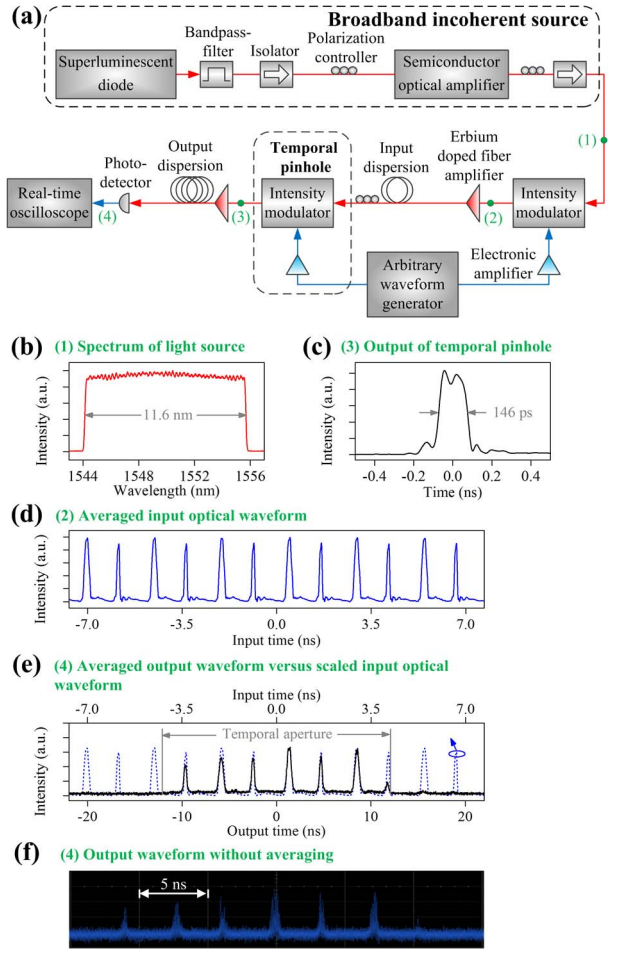

Fig. 3. Experimental setup and output waveforms along an incoherent temporal imaging (magnification) system. (a) Experimental setup. (b) Spectrum of the broadband incoherent-light source. (c) Optical output from the temporal pinhole. (d) Input optical temporal waveform. (e) Temporal intensity profile (solid black) of the output image compared with the scaled input temporal waveform (dashed blue), where the scaling between input time and output time is 2.86. All profiles in (b)–(e) are averaged for 256 times. (f) Temporal intensity profile of the output image without averaging.

12 GHz electronic amplifier. Figure 3(d) shows an example of an input temporal waveform, which is a periodic two-pulse sequence of Gaussian-like pulses. The two different consecutive pulses have FWHMs of 196 and 110 ps, respectively, and their time separation is 1.17 ns. The modulated light is sent through the input dispersive line (dispersion = –692 ps/nm), and the time-domain pinhole, which is realized by another 40 GHz electro-optic intensity modulator driven by an electronic pulsed waveform generated by the same arbitrary waveform generator, subsequently amplified by a 12.5 GHz electronic amplifier. Figure 3(c) shows the measured temporal pinhole, which has a nearly rectangular shape with an intensity FWHM of ~146 ps. After the temporal pinhole, the light is sent through the output dispersive line (dispersion = 1981 ps/nm) and is subsequently measured with a 45 GHz photodetector attached to a 28 GHz real-time oscilloscope. As shown in Fig. 3(e), the *averaged* output intensity waveform is a magnified temporal image of the input intensity waveform, with the expected magnification factor of $M = 2.86$, along the 8 ns (23 ns) input (output) temporal aperture. According to the theoretically expected temporal magnification factor, the intensity FWHM of the shortest pulse in the output temporal waveform, namely, the imaged version of the shortest input pulse, should be $\Delta T_{\mathrm{Out}} = |M|\Delta T_{\mathrm{In}} = 2.86 \times 110$ ps $\approx$ 315 ps. In the experiment, the measured intensity FWHM of the corresponding pulses in the output temporal waveform is ~345 ps, which, when compared with the ideal value, gives an input temporal resolution of $\delta\tau_{\mathrm{In}} \approx \sqrt{345^2 - 315^2}/|M|$ps $\approx$ 49.2 ps. The input resolution estimated from these measurements is in excellent agreement with the theoretical resolution of ~51 ps, leading to an experimental TBP of 162.6 (8 ns/49.2 ps).

The scheme demonstrated is particularly interesting for detection, measurement, or processing of high-speed RF waveforms. Photonic schemes providing similar capabilities have been demonstrated previously and applied widely, so-called optical temporal stretching systems [7,8,10,12]. The performance specifications (magnification, resolution, temporal aperture) of the incoherent-light temporal imaging configuration depend on the light source bandwidth and dispersion values, following a similar set of equations to those of standard (coherent) optical temporal stretching systems [7,8]. As a key advantage, the newly proposed configuration avoids the need for broadband coherent light pulse sources and precise pulse phase chirp. Nonetheless, a shortcoming of the incoherent method is that the output waveform exhibits a poor signal-to-noise ratio, such that averaging over multiple realizations is needed. The system could be upgraded for single-shot temporal imaging by using a suitable discrete-spectrum (multiwavelength) laser source, a strategy that has been demonstrated successfully for other incoherent-light temporal signal-processing operations [21].

In summary, we have demonstrated temporal imaging (magnification) of incoherent-light intensity waveforms using the time-domain equivalent of a spatial pinhole camera, avoiding the use of coherent-light processes, e.g., pulsed light sources. The setup demonstrated should prove particularly useful for temporal stretching of high-speed RF waveforms. This work could open the path for realization of a wide variety of critical instruments for measurement, generation, cloaking, and processing of high-speed electronic, RF, or optical signals in a very simple and practical fashion, by exploiting the ample wealth of knowledge developed for coherent temporal imaging and related platforms.

References

1. E. Treacy, IEEE J. Quantum Electron. **5**, 454 (1969).
2. B. H. Kolner, IEEE J. Quantum Electron. **30**, 1951 (1994).
3. C. V. Bennett and B. H. Kolner, IEEE J. Quantum Electron. **36**, 430 (2000).
4. R. Salem, M. A. Foster, and A. L. Gaeta, Adv. Opt. Photon. **5**, 274 (2013).
5. J. Azaña and M. A. Muriel, IEEE J. Sel. Top. Quantum Electron. **7**, 728 (2001).
6. J. van Howe, J. Hansryd, and C. Xu, Opt. Lett. **29**, 1470 (2004).
7. J. Azaña, N. K. Berger, B. Levit, and B. Fischer, J. Lightwave Technol. **24**, 2663 (2006).
8. Y. Han and B. Jalali, J. Lightwave Technol. **21**, 3085 (2003).
9. M. A. Foster, R. Salem, D. F. Geraghty, A. C. Turner-Foster, M. Lipson, and A. L. Gaeta, Nature **456**, 81 (2008).
10. K. Goda and B. Jalali, Nat. Photonics **7**, 102 (2013).
11. M. Fridman, A. Farsi, Y. Okawachi, and A. L. Gaeta, Nature **481**, 62 (2012).
12. J. Chou, O. Boyraz, D. Solli, and B. Jalali, Appl. Phys. Lett. **91**, 161105 (2007).
13. P. Naulleau and E. Leith, Appl. Opt. **34**, 4119 (1995).
14. V. Torres-Company, J. Lancis, and P. Andrés, J. Opt. Soc. Am. A **24**, 888 (2007).
15. C. Dorrer, Opt. Express **17**, 3341 (2009).
16. Y. Park and J. Azaña, Opt. Express **18**, 14752 (2010).
17. M. Young, Phys. Teach. **27**, 648 (1989).
18. B. H. Kolner, J. Opt. Soc. Am. A **14**, 3349 (1997).
19. Z. Wu, J. Dong, J. Hou, S. Yan, Y. Yu, and X. Zhang, Opt. Express **22**, 8076 (2014).
20. B. E. Saleh and M. C. Teich, *Fundamentals of Photonics* (Wiley, 1991), Chap. 10.
21. A. Malacarne, R. Ashrafi, M. Li, S. LaRochelle, J. Yao, and J. Azaña, Opt. Lett. **37**, 1355 (2012).